

## STOPPING POWER OF HEAVY IONS IN HOT DENSE PLASMAS\*

M. OGAWA, Y. OGURI, J. HASEGAWA, T. AOKI, U. NEUNER  
A. SAKUMI, K. NISHIGORI, K. SHIBATA, M. KOJIMA, M. YOSHIDA  
Y. NAKAJIMA

Research Laboratory for Nuclear Reactors, Tokyo Institute of Technology, Japan

M. NAKAJIMA AND K. HORIOKA

Department of Energy Sciences, Tokyo Institute of Technology, Japan

*(Received November 28, 2000)*

Energy loss of 6 MeV/ $u$   $^{56}\text{Fe}$  ions in a partially ionized helium plasma has been for the first time measured as a function of incident charge state ranging from 21+ to 25+. Enhancement of the energy loss of the ions in the discharge plasma has been observed over that in cold helium gas. The enhanced stopping of  $^{16}\text{O}$  ions with energies of  $\sim 0.2$  MeV/ $u$  in laser ablated LiH plasma has been also observed over that in cold matter. Theoretical calculation proposed by Sigmund reproduces the energy dependence of the experimental stopping power of the  $^{16}\text{O}$  ions in the plasma.

PACS numbers: 34.50.Bw, 52.20.Hv, 52.40.Mj, 52.50.Jm

### 1. Introduction

Stopping power of heavy ions in dense plasmas plays an important role in heavy ion inertial fusion where energy of driver beam is converted to X-ray energy in indirect irradiation targets. In this scenario, it is important to study ion stopping near the Bragg peak in range distribution where the energy dependence of stopping power also exhibits a peak. We focus our interest on experiments with heavy ions having energies near the peak in the stopping power curve. Many experiments of heavy-ion stopping in the completely ionized hydrogen plasmas formed by  $Z$ -pinch discharge have been carried out by GSI [1–6] and Orsay [7,8] groups. They observed the enhanced

---

\* Presented at the XXXV Zakopane School of Physics “Trends in Nuclear Physics”, Zakopane, Poland, September 5–13, 2000.

stopping of ions in the plasmas compared with that in the cold matter. Jacoby *et al.* have observed the largest enhancement factor of 35 for 45 keV/*u* krypton ions [5]. On the other hand, no plasma effect was obvious in the partially ionized argon plasma of low degree of ionization [9] which contained many bound electrons. We have studied stopping power of 6 MeV/*u* iron ions in a partially ionized plasma of helium which includes the bound and free electrons with nearly equal weight. The stopping power of fast heavy ions in plasma is expressed by the following Bethe type equation [10–12].

$$-\frac{dE}{dX} = -\frac{4\pi Z_{\text{eff}}^2 e^4}{mv^2} \left[ N_{\text{be}} \ln \left( \frac{2mv^2}{I_{\text{av}}} \right) + N_{\text{fe}} \ln \left( \frac{2mv^2}{\hbar\omega_p} \right) \right], \quad (1)$$

where  $m$  is the electron mass,  $Z_{\text{eff}}$  and  $v$  are, respectively, the effective charge and the velocity of the projectile ion,  $N_{\text{be}}$  and  $N_{\text{fe}}$  are, respectively, the number densities of bound electron and free electron, and  $I_{\text{av}}$  and  $\omega_p$  are, respectively, the average ionization energy of target atom and the plasma frequency. The charge equilibration of the projectile ions plays an important role in the stopping process. So we measure the energy loss of the iron ions as a function of projectile charge state.

On the other hand, Sigmund has proposed an equation extended from the Bohr type equation to analyze the stopping power of low-energy ions with velocity near or below the Bohr velocity [13]. The Sigmund equation can be modified for the plasma as below.

$$-\frac{dE}{dX} = -\frac{4\pi Z_{\text{eff}}^2 e^4}{mv^2} \left[ N_{\text{be}} L \left( \frac{mv^3}{Z_{\text{eff}} e^2 \omega} \right) + N_{\text{fe}} L \left( \frac{mv^3}{Z_{\text{eff}} e^2 \omega_p} \right) \right], \quad (2)$$

where  $\omega$  is the resonance frequency of bound electron and  $L$  is the stopping number given by Sigmund.

It is interesting to test the Sigmund equation. So we investigate the stopping power as a function of projectile energy in the energy region near and/or below the Bragg peak. For this measurement we use target plasmas formed by laser irradiation to prevent the projectile-beam deflection from the magnetic field.

## 2. Experiments

### 2.1. High-energy ions in helium discharge plasma

The experiments for heavy-ion beams with energy higher than the Bragg peak were carried out at HIMAC (Heavy Ion Medical Accelerator at Chiba) of NIRS (National Institute of Radiological Sciences). To ensure the enough interaction length, the target plasma was formed by the  $Z$ -pinch discharge of helium gas in a quartz discharge tube of 165 mm in length and 27 mm

in inner diameter [14,15]. The plasma target was differentially pumped to maintain the vacuum of accelerator beam line. A pair of apertures of 2 mm in diameter were placed on both ends of the discharge tube to define the beam-plasma interaction area. The  $Z$ -pinch discharge was driven with a capacitor of 4  $\mu\text{F}$  at voltage of 18 kV. The discharge current rose to a peak of 60 kA at  $t = 2 \mu\text{s}$ . The helium gas pressure was adjusted to 120 and 200 Pa. The electron density was deduced from the Stark broadening of He II  $n = 4$  to  $n = 3$  line at 468.6 nm [16]. The electron temperature was deduced from the line-intensity ratio of  $I(\text{He II } 468.6 \text{ nm})/I(\text{He I } 587.6 \text{ nm})$  [17]. The general behavior of the helium plasma was simulated with the MULTI-Z code [14] which was extended by one of the authors, T. Aoki, from the original 1D hydrodynamics code of MULTI [18] to include the MHD components.

Fig. 1 compares the measured and simulated electron densities for the gas pressure of 120 and 200 Pa. The measured electron density ranges from  $1 \times 10^{18}$  to  $2 \times 10^{18} \text{ cm}^{-3}$  and from  $2 \times 10^{18}$  to  $4 \times 10^{18} \text{ cm}^{-3}$  for the gas pressure of 120 and 200 Pa, respectively, during the first pinch around  $t = 1 \mu\text{s}$ . On the other hand, the electron temperature does not so fluctuate as the electron density and varies between 4 and 5 eV. The complete LTE (Local Thermal Equilibrium) condition for helium plasma gives an electron density of  $n_e > 1 \times 10^{18} \text{ cm}^{-3}$  at  $T_e = 4 \text{ eV}$  with a time scale of  $\tau = 0.1 \mu\text{s}$  [17]. So the present helium plasma fulfills almost the LTE condition. However, it should be noted that the discharge plasma is applicable as a target only around  $t = 1 \mu\text{s}$ . This is because the uniform plasma was observed with a streak camera only between  $t = 0.9$  and  $1.3 \mu\text{s}$  when the gas pressure was set to 120 Pa. The spatial distribution of the electron density was calculated with the MULTI-Z code to examine the uniformity of the discharge plasma target.

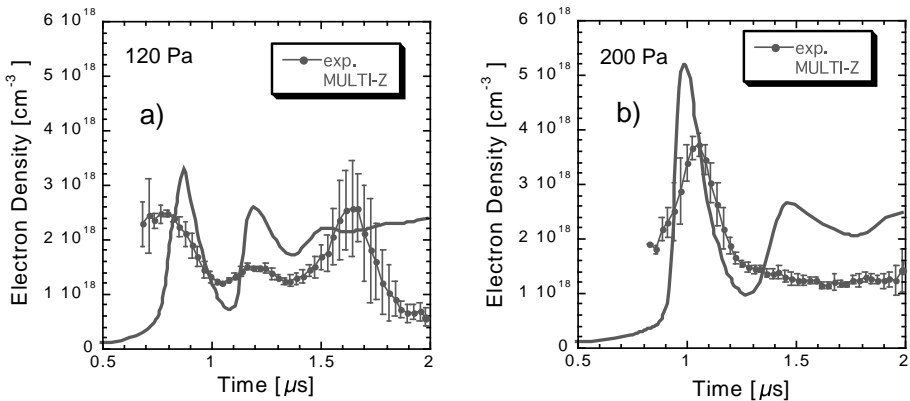


Fig. 1. Time evolution of electron densities measured and calculated with MULTI-Z code, (a) for 120 Pa and (b) for 200 Pa.

The calculation provided the spatial non-uniformity of the plasma as  $\pm 20\%$  within a radius of 1 mm for the gas pressure of 200 Pa. The non-uniformity for the case of 120 Pa was  $\pm 10\%$ . The MULTI-Z calculation indicated that the present plasma target was uniform enough for the in-beam experiments with the beam radius defined as 1 mm.

The energy loss experiments were performed with an  $^{56}\text{Fe}$  beam of 6 MeV/ $u$  energy at HIMAC. The pulsed iron beam had a time spacing of 10 ns. The  $^{56}\text{Fe}$  ions with selected charge states ranging from 21+ to 25+ were injected to the target plasma. The energy loss of the ions having passed through the plasma was measured with the time of flight method. The flight distance was 3.8 m. The outgoing ions were detected with an assembly of a gold foil and a micro channel plate (MCP). The MCP placed at the angle of 45 degrees to the ion beam detected the secondary electrons generated at the gold foil. The MCP was shielded from the plasma light. Fast digital oscilloscopes recorded the signals of MCP, RF, beam pickup and discharge current. The measurements were repeated for various timings after discharge ignition.

In order to convert the measured energy loss to the stopping power, the mass thickness  $dX$  of the target plasma was evaluated as  $dX = M_{\text{He}}Ln_e/\langle Z \rangle$ , where  $M_{\text{He}}$ ,  $L$ ,  $n_e$ ,  $\langle Z \rangle$  are the mass of helium atom, the plasma length, the electron density and the mean charge of helium plasma, respectively. The experimental mean charge was evaluated by inserting the measured electron density and temperature into the Saha's equation [19]. The MULTI-Z code also gave the mean charge  $\langle Z \rangle$ . Fig. 2 compares the experimental mean charge and the simulated one. We adopted the experimental values to calculate the plasma mass thickness although the discrepancy between

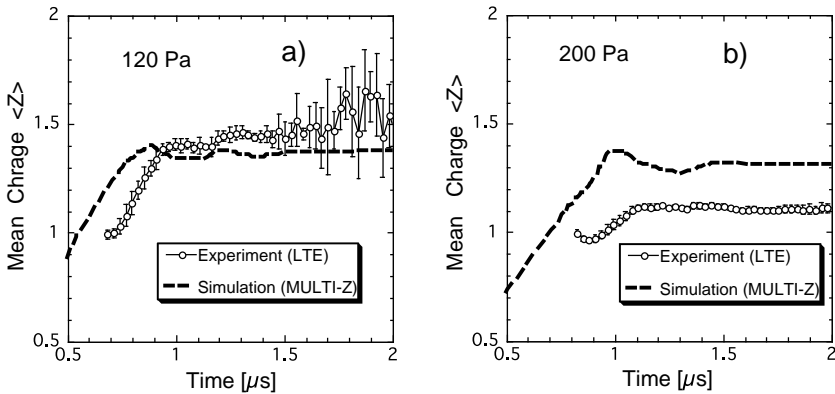


Fig. 2. Time evolution of electron temperature measured and calculated with MULTI-Z code, (a) for 120 Pa and (b) for 200 Pa.

the experimental and simulated ones, in particular, for the case of 200 Pa is obvious. For example, the electron density of  $n_e = 1 \times 10^{18} \text{ cm}^{-3}$  and the mean charge of  $\langle Z \rangle = 1$  give the mass thickness of  $dX = 55 \mu\text{gcm}^{-2}$  for the plasma column of 165 mm in length. The equilibrium thickness  $X$  of the carbon foil was obtained by Baron [20] as  $X = 5.9 + 22.4W - 1.13W^2$  where the thickness  $X$  and the ion energy  $W$  are in  $\mu\text{gcm}^{-2}$  and MeV/ $A$ , respectively. This empirical formula gives the thickness of  $100 \mu\text{gcm}^{-2}$  which was almost fulfilled by the helium plasma with the gas pressure of 200 Pa at the first pinch around  $t = 1 \mu\text{s}$ .

## 2.2. Low-energy ions in laser plasma

Experiments with the low-energy ions were conducted to study the stopping process for the ion energy lower than the Bragg peak. The  $^{16}\text{O}$  beams with energy ranging from 2.4 to 5.6 MeV are generated with the 1.7 MV tandem at Tokyo Institute of Technology. A proton beam with the same velocity as the oxygen beam is also used to extract the Coulomb logarithm terms in the stopping power equation. Two types of plasma targets are installed on the beam line. One is based on a Nd-glass laser of 3 J energy and 30 ns pulse width [21–23]. A LiH pellet of about 60  $\mu\text{m}$  in diameter is irradiated by the laser. The spherically expanding plasma was observed with a fast framing camera. The electron density was diagnosed by the Mach–Zehnder interferometry. Fig. 3 indicates radial distributions of the electron density observed at 60, 80 and 100 ns after start of the laser irradiation. The LiH plasma with the electron density of  $1 \times 10^{18} \text{ cm}^{-3}$  at  $t = 60$  ns is appropriate to an incident beam with a radius of 0.5 mm. The optical spectroscopy of the continuum emission gave the electron temperature of 10 to 20 eV. The ratios of singly ionized atom to neutral atom were evaluated for hydrogen and lithium using the Saha's equation [19]. The ratios of the number densities were  $n(\text{Li}^+)/n(\text{Li}) \geq 1000$  and  $n(\text{H}^+) = 390$ . The ratio of  $\text{Li}^{2+}$  to  $\text{Li}^+$  was  $n(\text{Li}^{2+})/n(\text{Li}^+) = 0.1$  even for the minimum density for the LTE condition, *i.e.*,  $10^{20} \text{ cm}^{-3}$ . Consequently the LiH plasma consisted of mainly of  $\text{Li}^+$  and  $\text{H}^+$  and the neutral component was negligible. The mass thickness of the LiH plasma was evaluated as  $\Delta X = 1.4 \mu\text{gcm}^{-2}$  at  $t = 60$  ns. The energy loss of the ions in the LiH plasma was measured with the time-of-flight method where the DC beam from the tandem was pulsed by a 100 MHz chopper. The ions having passed through the plasma were detected with an assembly consisting of a carbon foil and a MCP. The secondary ions emitted from the carbon foil were bent by 180 degrees with a permanent magnet and then detected by the MCP. This detector geometry was adopted to shield the MCP from the plasma light.

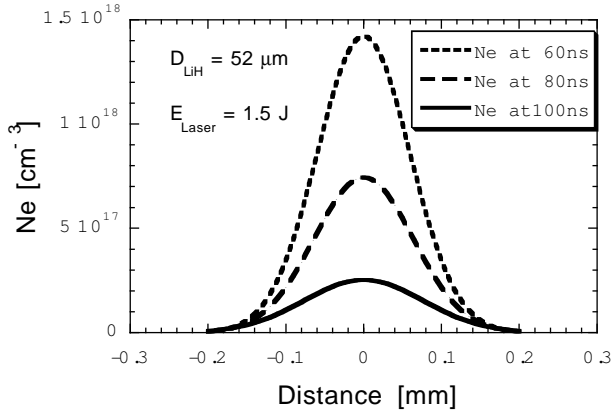


Fig. 3. Radial distributions of electron density of LiH plasma observed at 60, 80 and 100 ns after the laser irradiation.

### 2.3. Solid hydrogen target for laser plasma

Another plasma target is formed by irradiating a plate with a CO<sub>2</sub> laser of 6 J per pulse. The laser is line-focused to suppress the density gradient along the incident ion trajectory. We replace the previous polyethylene target with a solid hydrogen target to improve the degree of ionization of the plasma. Fig. 4 shows a schematic view of the solid hydrogen target for the ion-plasma interaction experiment. We use a GM refrigerator with the refrigerating power of 1 W at temperature of 4 K. The hydrogen gas is fed to an ice forming cell covered with an acrylic case after a copper bed is cooled down to 7 K from the room temperature in 60 min. It takes 10 min to grow a transparent hydrogen ice of 8 mm × 3 mm × 4 mm in thickness. This size

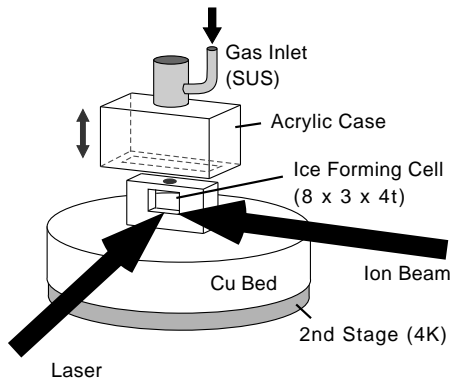


Fig. 4. A schematic view of solid hydrogen formation for ion-plasma interaction.

of the ice is adjusted to the line-focused CO<sub>2</sub> laser spot. The hydrogen ice can be formed every 10 min without breaking the vacuum. The hydrogen plasma was diagnosed by the optical spectroscopy. The plasma emission at a distance between 0 and 3 mm from the hydrogen surface was collected with an optical fibre connected to a polychromator. The electron density was deduced from the Stark broadening of the H<sub>β</sub> lines and the electron temperature from the intensity ratio of the H<sub>α</sub> to the H<sub>β</sub> line [17]. Fig. 5 shows the time evolution of the electron density, the electron temperature and the CO<sub>2</sub> laser. The present electron density of  $0.5 \sim 2 \times 10^{17} \text{ cm}^{-3}$  is lower by a factor of two than the electron density measured previously with the polyethylene plasma. This discrepancy is probably due to the larger objective area than the previous one which was defined to a distance of 0.5 to 1.5 mm.

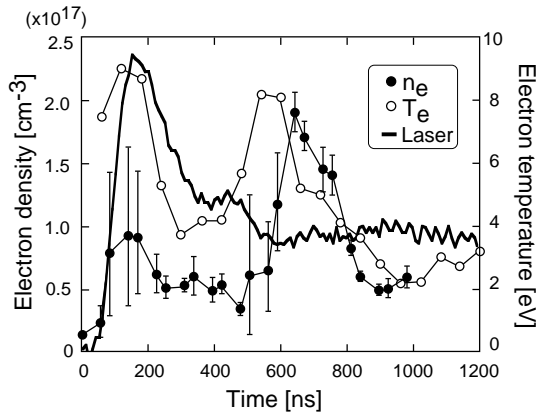


Fig. 5. Time profiles of electron density and electron temperature of hydrogen plasma, and CO<sub>2</sub> laser.

### 3. Results

#### 3.1. High-energy ions in helium discharge plasma

Fig. 6 shows the measured stopping power of <sup>56</sup>Fe ions in the helium plasma formed with the gas pressure of 120 Pa where the errors of  $\pm 30$  to 60 % are not indicated for simplicity. The charge states of the incident iron ions ranges from 21+ to 25+ where the first pinch is around 1  $\mu$ s after the ignition. In this case the stopping power depends on the charge state because the plasma thickness was less than the equilibrium thickness of about 100  $\mu\text{gcm}^{-2}$ . The stopping power observed in the plasma around 1.1  $\mu$ s is enhanced by a factor of two to three than the stopping power for the cold helium gas [24] as indicated in Fig. 6 with a dotted line. The theoretical

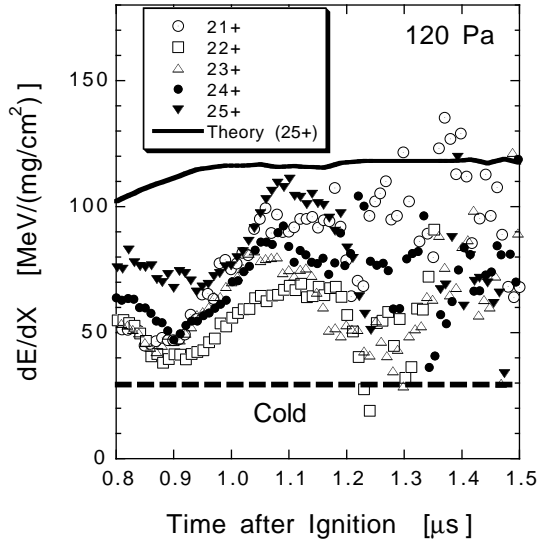


Fig. 6. Stopping power of 6 MeV/ $u$   $^{56}\text{Fe}$  ions in helium plasma measured for gas pressure of 120 Pa as a function of incident charge state. A dotted line indicates stopping power for cold helium gas and a solid line depicts theoretical stopping power of  $^{56}\text{Fe}$  ions with charge state of 25 in helium plasma.

stopping power calculated with the Bethe type of Eq. (1) is also depicted in the figure by assuming the effective charge of the  $^{56}\text{Fe}$  ions as 25+. The theoretical curve overlaps with the highest stopping power observed at the pinch timing although the theoretical evaluation does not reproduce the obvious time dependence of the experimental data. However, it should be noted that the conversion of the experimental energy loss to the stopping power depends on the mean charge  $\langle Z \rangle$  of the helium plasma. This discrepancy might be removed by taking into account of the time evolution of the effective charge and by the more detailed plasma diagnostics. The plasma diagnostics with the higher spatial resolution could give the more reliable estimation of the mean charge  $\langle Z \rangle$  of the partially ionized helium plasma.

Fig. 7 shows the similar results for the case of 200 Pa. The measured stopping power is independent of the initial charge state of the  $^{56}\text{Fe}$  ions within the errors. This fact reflects that the charge state of the projectile ions reached to the equilibrium distribution in the plasma and then the major part of the stopping process was governed by the equilibrium charge state. In this case the target plasma was thick enough to realize the charge-state equilibrium. The enhanced stopping over the cold helium gas was clearly observed for the 6 MeV/ $A$   $^{56}\text{Fe}$  ions in the plasma.

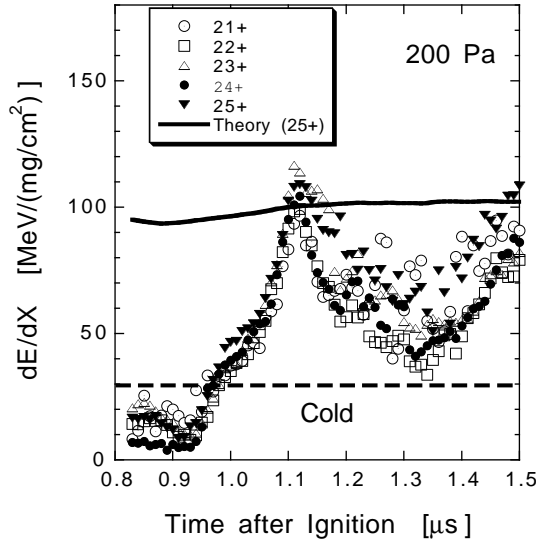


Fig. 7. Stopping power of 6 MeV/u  $^{56}\text{Fe}$  ions in helium plasma measured for gas pressure of 200 Pa as a function of incident charge state. A dotted line indicates stopping power for cold helium gas and a solid line depicts theoretical stopping power of  $^{56}\text{Fe}$  ions with fixed charge state of 25 in helium plasma.

3.2. Low-energy ions in laser plasma

Fig. 8 compares the stopping power measured as a function of the  $^{16}\text{O}$  beam energy with the compiled values for the cold matter [25]. It is first noted that the experimental values are larger by a factor of two to three than the curve for the cold matter. The experimental stopping power increases with the decrease of the beam energy. On the contrary, the stopping power

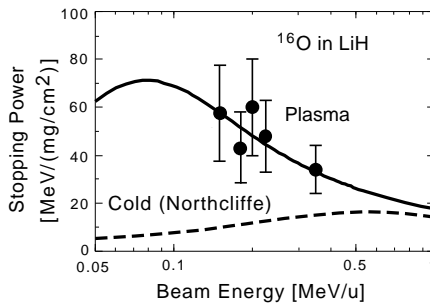


Fig. 8. Stopping power of  $^{16}\text{O}$  ions in LiH plasma measured as a function of beam energy. A dotted line indicates stopping power tabulated for cold matter. A solid line depicts theoretical stopping power based on the Sigmund's work [13].

curve for the cold matter decreases in the energy region of below  $0.5 \text{ MeV}/u$ . This fact led us to use the Eq. (2) instead of the Bethe type Eq. (1) for the theoretical calculation of the stopping power.

To calculate the theoretical stopping power of the ions in the plasma, we estimated the charge-state fraction of the incident ions in the target plasma by solving the rate equation [11]. As a typical case, the effective charge was obtained to be 4.7 for the  $3.6 \text{ MeV } ^{16}\text{O}$  ions in the LiH plasma with the electron density of  $n_e = 1 \times 10^{18} \text{ cm}^{-3}$  and the electron temperature of  $T_e = 15 \text{ eV}$ . The Coulomb logarithm term in the Eq. (2) was taken from the calculation by Sigmund [13]. The theoretical stopping power for the plasma is indicated with a solid curve in Fig. 8. The calculation reproduced the energy dependence and also the magnitude of the measured stopping power. This calculation suggests the larger stopping power for the lower-energy beam in a fully ionized plasma. In fact Jacoby *et al.* have observed the large enhancement factor of 35 [5].

#### 4. Summary

Stopping power of  $6 \text{ MeV}/u$   $^{56}\text{Fe}$  ions in a partially ionized helium plasma produced by *Z*-pinch discharge has been for the first time measured as a function of incident-beam charge state ranging from 21+ to 25+. We have observed that the stopping power measured around the pinch timing at  $t = 1.1 \mu\text{s}$  is larger by a factor of two to three than the stopping power for cold helium gas. However, further detailed study is necessary to analyze the time evolution of the stopping process.

The stopping power of low-energy  $^{16}\text{O}$  ions in LiH plasma has been for the first time observed as a function of beam energy. Enhancement factors of the stopping power for the plasma over that for the cold matter are two to three depending on the beam energy. Theoretical calculation based on the work of Sigmund is in good agreement with the experimental energy dependence of stopping power.

This work was partially supported by Grant-in-Aid for Scientific Research of the Japanese Ministry of Education, Science, Sport and Culture, and the Research Project with Heavy Ions at NIRS-HIMAC. One of the authors (U.N.) was supported by the A.V. Humboldt-Stiftung and by the Japan Society for the Promotion of Science. C. Deutsch is acknowledged for valuable discussions.

## REFERENCES

- [1] D.H.H. Hoffmann, J. Meyer-ter-Vehn, R.W. Mueller, I. Hofmann, R. Bock, R. Arnold, *Nucl. Instrum. Methods* **A278**, 44 (1989).
- [2] D.H.H. Hoffmann, K. Weyrich, H. Wahl, D. Gardés, R. Bimbot, C. Fleurier, *Phys. Rev.* **A42**, 2313 (1990).
- [3] E. Boggasch, J. Jacoby, H. Wahl, K.G. Dietrich, D.H.H. Hoffmann, W. Laux, M. Elfers, C.R. Haas, V.P. Dubenkov, A.A. Golubev, *Phys. Rev. Lett.* **66**, 1705 (1991).
- [4] K.G. Dietrich, D.H.H. Hoffmann, E. Boggasch, J. Jacoby, H. Wahl, M. Elfers, C.R. Haas, V.P. Dubenkov, A.A. Golubev, *Phys. Rev. Lett.* **69**, 3623 (1992).
- [5] J. Jacoby, D.H.H. Hoffmann, W. Laux, R.W. Müller, H. Wahl, K. Weyrich, E. Boggasch, B. Heimrich, C. Stöckl, H. Wetzler, S. Miyamoto, *Phys. Rev. Lett.* **74**, 1550 (1995).
- [6] C. Stöckl, M. Roth, W. Süß, H. Wetzler, W. Seelig, M. Kulish, P. Spiller, J. Jacoby, D.H.H. Hoffmann, *Fusion Technol.* **31**, 169 (1997).
- [7] D. Gardes, R. Bimbot, M.F. Rivet, A. Servajean, A. Fleurier, D. Hong, C. Deutsch, G. Maynard, *Laser Part. Beams* **8**, 575 (1990).
- [8] A. Servajean, D. Gardes, R. Bimbot, M. Dumail, B. Kubica, A. Richard, M.F. Rivet, C. Fleurier, D. Hong, C. Deutsch, G. Maynard, *J. Appl. Phys.* **71**, 2587 (1992).
- [9] H. Wetzler, W. Suess, C. Stoeckl, A. Tauschwitz, D.H.H. Hoffmann, *Laser Part. Beams*, **15**, 449 (1997).
- [10] T.A. Mehlhorn, *J. Appl. Phys.* **52**, 6522 (1981).
- [11] T. Peter, J. Meyer-ter-Vehn, *Phys. Rev.* **A43**, 1998 and 2015 (1991).
- [12] C. Couillaud, R. Deicas, Ph. Nardin, M.A. Beuve, J.M. Guihaumé, M. Renaud, M. Cukier, C. Deutsch, G. Maynard, *Phys. Rev.* **E49**, 1545 (1994).
- [13] P. Sigmund, *Phys. Rev.* **A54**, 3113 (1996).
- [14] T. Hosokai, M. Nakajima, O. Iwase, T. Nakamura, T. Endou, K. Fujii, T. Aoki, K. Horioka, T. Kohno, Y. Oguri, T. Murakami, S. Miyamoto, M. Ogawa, *Fusion Eng. Des.* **32-33**, 551 (1996).
- [15] M. Ogawa, U. Neuner, H. Kobayashi, Y. Nakajima, K. Nshigori, K. Takayama, O. Iwase, M. Yoshida, M. Kojima, J. Hasegawa, Y. Oguri, K. Horioka, M. Nakajima, S. Miyamoto, V. Dubenkov, T. Murakami, *Laser Part. Beams* in press.
- [16] A. Gawron, S. Maurmann, F. Böttcher, A. Meckler, H.J. Kunze, *Phys. Rev.* **A38**, 4737 (1988).
- [17] H.R.T. Griem, *Plasma Spectroscopy*, McGraw-Hill, New York 1964.
- [18] R. Ramis, R. Schmalz, J. Meyer-ter-Vehn, *Comput. Phys. Commun.* **49**, 475 (1988).
- [19] R.O. Dendy, *Plasma Physics*, Cambridge University Press, 1993.
- [20] E. Baron, *IEEE Trans. Nucl. Sci.* **NS-26**, 2411 (1979).

- [21] A. Sakumi, H. Okazaki, T. Watanabe, K. Shibata, H. Fukuda, U. Neuner, S. Garnsomsart, M. Ogawa, Y. Oguri, *Nucl. Instrum. Methods* **A415**, 648 (1998).
- [22] Y. Oguri, S. Abe, A. Sakumi, H. Okazaki, T. Watanabe, K. Shibata, K. Nishigori, M. Ogawa, *Nucl. Instrum. Methods* **A415**, 657 (1998).
- [23] A. Sakumi, T. Watanabe, K. Shibata, J. Hasegawa, M. Ogawa, Y. Oguri, *J. Nucl. Sci. Technol.* **36**, 326 (1999).
- [24] J.F. Ziegler, J.P. Biersack, U. Littmark, *The Stopping and Range of Ions in Solids*, Pergamon, New York 1985.
- [25] L.C. Northcliffe, R.F. Schilling, *Nucl. Data Tables* **A7**, 233 (1970).